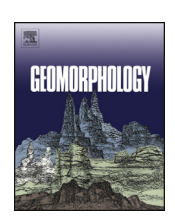
ELSEVIER

Contents lists available at ScienceDirect

Geomorphology

journal homepage: www.elsevier.com/locate/geomorph



Backwater controls on the evolution and avulsion of the Qingshuigou channel on the Yellow River Delta



Shan Zheng a,*, Douglas A. Edmonds b,d, Baosheng Wu c, Shasha Han a

- ^a State Key Laboratory of Water Resources and Hydropower Engineering Science, Wuhan University, Hubei 430072, China
- ^b Department of Earth and Atmospheric Sciences, Indiana University, Bloomington, IN 47405, USA
- ^c State Key Laboratory of Hydroscience and Engineering, Tsinghua University, Beijing 100084, China
- ^d Center for Geospatial Data Analysis, Indiana University, Bloomington, IN 47405, USA

ARTICLE INFO

Article history: Received 4 October 2018 Received in revised form 17 February 2019 Accepted 22 February 2019 Available online 25 February 2019

Keywords:
Qingshuigou channel
Yellow River Delta
Hydrodynamic and morphodynamic backwater
Erosion and deposition processes

ABSTRACT

As rivers approach base level, their water and sediment dynamics are affected by a transitional reach known as the backwater zone. At low flows, backwater zones cause flow deceleration and in-channel sedimentation, but at high flows, they cause flow acceleration and erosion. Over many floods, the dynamics of deposition and erosion in the backwater zone are thought to control the locations of avulsions on some large deltaic channels. However, in various studies, the role of the backwater is often inferred or modeled, and directly observed evidence of how backwater affects channel dynamics at avulsion sites remains scarce. In this study, we show how the backwater zone impacts the evolution and avulsion of the Qingshuigou channel, a recent lobe on the Yellow River Delta, using four decades (1976-2015) of data from systematic surveys of water discharge, sediment load, crosssectional profiles and water surface elevation. The results show that the channel was commonly eroded during flood seasons and aggraded during nonflood seasons. Erosion rates generally decreased in the downstream direction along the lower channel reach during flood seasons, primarily due to downstream channel widening and the subsequent decrease in sediment transport capacity. The erosion rate reached zero at the cross-sections farthest downstream, which is contrary to expectations under hydrodynamic backwater effects, where drawdown causes erosion to increase downstream during high flows. During nonflood seasons, maximum sedimentation occurred upstream of the backwater zone, possibly due to impacts of local topography of meandering bends or constriction from dikes. Morphodynamic backwater accompanied by the deposition and gradual progradation of a mouth bar resulted in downstream increasing sedimentation, superelevation, and lateral migration rates along the lower channel reach from 1985 to 1996. The predicted avulsion location was near cross-sections 06 or 07 with an avulsion length of ~20–30 km upstream of the shoreline, which was consistent with those for historical avulsions. We emphasize the close interplay between backwater effects and channel geometry and argue that morphodynamic backwater may play a more important role than hydrodynamic backwater in setting up and triggering avulsions on the Yellow River Delta.

© 2019 Elsevier B.V. All rights reserved.

1. Introduction

When a river approaches a body of standing water, its water surface gradually changes slope to match the water surface elevation at the outlet. This gradual change causes a transition from normal to gradually varying flow, which leads to flow deceleration (or acceleration) near the outlet. This section of the river is typically referred to as the backwater zone, and may extend many hundreds of kilometers upstream of the outlet on large lowland rivers (Nittrouer et al., 2012; Lamb et al., 2012; Ganti et al., 2016). Interestingly, two types of backwater zones are recognized. Hydrodynamic backwater is caused by nonuniform flow

dynamics, whereas morphodynamic backwater is caused by migrating sediment bed waves.

Hydrodynamic backwater can influence sediment erosion and deposition, and has been proposed to control avulsion locations on deltas (Jerolmack and Swenson, 2007; Chatanantavet et al., 2012). Spatially, backwater hydrodynamics tend to create flow deceleration and sediment deposition during low flows and flow acceleration and erosion during high flows. However, over time, these changes are not equally balanced, and net aggradation tends to occur in the upstream portions of backwater zones (Fig. 1B, Chatanantavet et al., 2012; Lamb et al., 2012; Nittrouer et al., 2012; Ganti et al., 2016). For example, studies on the hydrodynamic backwater effects of the lower Mississippi River have shown that spatial and temporal divergence in sediment transport leads to aggradation in the upstream portion and degradation in the

^{*} Corresponding author. E-mail address: zhengs@whu.edu.cn (S. Zheng).

(A) Morphodynamic backwater

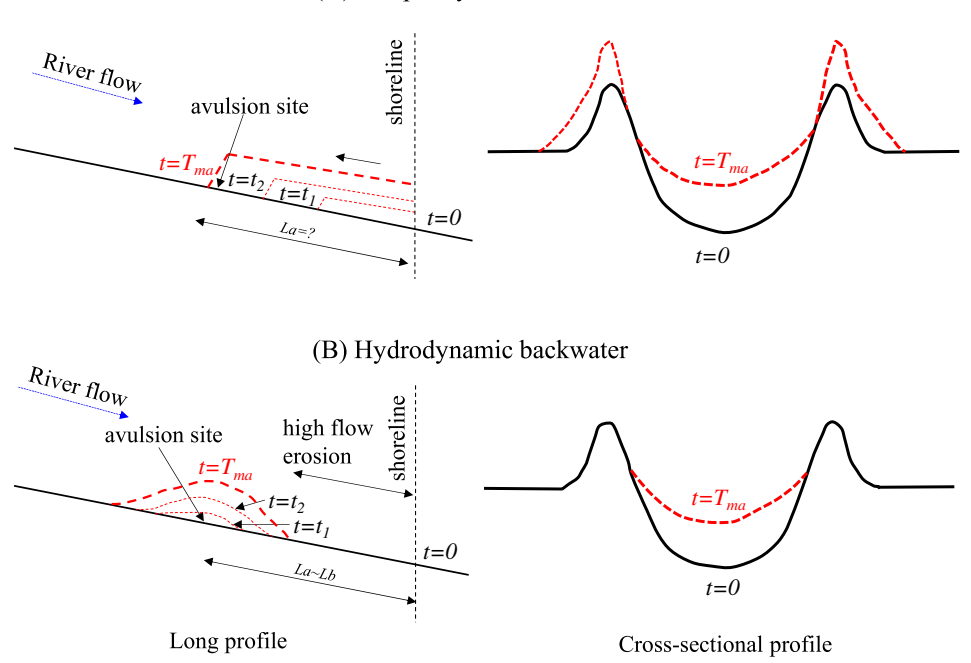


Fig. 1. Schematic summary of the existing theory of (A) morphodynamic backwater and (B) hydrodynamic backwater for avulsion cycles (after Ganti et al., 2016). Note black lines show the original channel boundary and the red dashed lines show the channel boundary altered by backwater-triggered aggradation. The left figures show channel long profile and the right ones show cross-sectional profile. Morphodynamic backwater results in an upstream migrating wave of aggradation and in-channel backfilling that initiates near the shoreline as a result of mouth bar progradation. The channel bed and the levees aggrade resulting in channel superelevation and setting up for avulsion. Under hydrodynamic backwater effects, in-channel sedimentation formed within the upstream portion of the backwater zone due to preferential erosion caused by the floods in the downstream portion of the backwater zone. The channel bed aggrades at the avulsion site but levees do not aggrade significantly because the variable flows within the backwater zone are accommodated by changing water surface slope with little changes in water stage height that may result in overbank deposition (Ganti et al., 2016).

downstream portion of the backwater reach (e.g., Chatanantavet et al., 2012; Lamb et al., 2012; Nittrouer et al., 2012). Aggradation in the upper reaches is thought to create superelevation and river avulsion. Indeed, this idea is supported by data showing that the distance from the avulsion location of the Mississippi River Delta to the shoreline approximately scales with a characteristic backwater length, indicating the important role played by hydrodynamic backwater effects in facilitating channel avulsions that lead to the formation of fluvial distributary channels (Jerolmack and Swenson, 2007; Chatanantavet et al., 2012; Lamb et al., 2012; Nittrouer et al., 2012).

Different from the classic use of the term "backwater" resulting from nonuniform flow hydrodynamics, morphodynamic backwater effects were defined by Hoyal and Sheets (2009) to include channel backfilling or the upstream migrating wave of sediment deposition accompanied by the gradual progradation of a mouth bar (Fig. 1A, Ganti et al., 2016). Channel backfilling caused by these downstream-mediated topographic effects or morphodynamic backwater effects may dominate upstream avulsion processes and control surface mechanics and stratigraphy (Hoyal and Sheets, 2009). For example, studies have documented channel backfilling preceding avulsion in the field, e.g., the Ovens and King Rivers in Australia (Schumm et al., 1996), the Kosi River in India (Sinha, 2009; Sinha et al., 2014) and the Diaokouhe channel of the Yellow River Delta (YRD) in China (Shi and Zhang, 2003; note that the Qingshuigou channel replaced the Diaokouhe channel to transport water and sediment to the sea after an avulsion in 1976). Channel backfilling caused by morphodynamic backwater effects has also been observed in avulsion cycles of channels in flume experiments (e.g., Edmonds et al., 2009; Hoyal and Sheets, 2009; van Dijk et al., 2009) and numerical modeling (e.g., Reitz et al., 2010).

Despite many studies on the YRD, the role of the backwater zone in driving the avulsion process is unknown (e.g. Wang and Liang, 2000; Bi et al., 2014; Zhou et al., 2015; Zheng et al., 2017, 2018). This fact is surprising given that frequent avulsions have played a significant role in

distributing sediment on the YRD and forming the North China Plain. The Qingshuigou channel, the recent lobe on the YRD, has been maintained for approximately four decades, a time period that greatly exceeds the average lifespan of abandoned lobes on the delta (~10 years, Wang and Liang, 2000; Wang, 2010). Shi and Zhang (2003) proposed an avulsion cycle based on the evolution of the Diaokouhe and Oingshuigou channels, i.e., sediment is deposited downstream of the avulsion point in new channels, which have relatively low bed elevations, following avulsions, and a single channel gradually forms by scouring the previous deposits. As a delta lobe extends basinward, the channel gradient decreases and backfilling begins, forcing water to leave the confined channel and trigger avulsion. Hydrodynamic backwater effects were not considered in the proposed avulsion cycle. Zheng et al. (2018) argued that the evolution of the lower Qingshuigou channel was characterized by four phases: I (1976-1980) rapid aggradation; II (1980-1985) channel widening and enlargement; III (1985-1996) main channel aggradation and backfilling; and IV (1996-2015) main channel incision and deepening. The influence of backwater hydrodynamics on channel evolution processes was also not considered.

Few studies can quantify how the backwater zone affects channel evolution and avulsion dynamics because of the difficulty in witnessing and measuring avulsion events. Therefore, we investigated the morphodynamic and hydrodynamic backwater impacts in the Qingshuigou channel. A rich database has been provided by the Yellow River Conservation Commission (YRCC), including systematic surveys of water discharge, sediment load, cross-sectional profiles and water surface elevation from 1976 to 2015. With these data, we focus on answering the following questions: 1) How do backwater zones impact sediment transport and evolution processes in the Qingshuigou channel? 2) Is there a quantifiable signature of backwater effects setting up and triggering avulsions on the YRD? Answers to these questions are important for understanding and predicting the evolution of the

Qingshuigou channel and may inform the development and management of the YRD, where large populations reside.

2. Study area

The Yellow River estuary is dominated by fluvial processes with a length of tidal limit <20 km and tide range of \sim 1 m (Wang and Liang, 2000). The modern YRD began to develop in 1855 when the lower Yellow River migrated from south to north to join the Bohai Sea (Fig. 2A), and massive sections of land have accreted since then. Avulsions have occurred \sim 11 times during 1855–1976, and the average lifespan of the deltaic channel is only \sim 10 years. Readers who are interested in historical avulsions on the delta are referred to Wang and Liang (2000), Wang (2010) and Zheng et al. (2017, 2018).

The most recent avulsion occurred in 1976, when the river flow was artificially diverted from the Diaokouhe channel to the Qingshuigou channel. The initial bed elevation at the excavated Qingshuigou channel was much lower than that of the abandoned Diaokouhe channel (Wang, 2010). River flow shifted frequently downstream of the avulsion point and the main channel became single-thread and relatively stable after ~1980 (Wang and Liang, 2000; Zheng et al., 2018). Since then, the Qingshuigou channel has experienced many disturbances (Table 1). Water was artificially diverted to a new excavated channel in the lower Qingshuigou channel in 1996 to enhance land accretion near an offshore oil platform (Wang and Liang, 2000). The channel reach downstream of the Q8 cross-section was artificially blocked (Fig. 2B). The

channel bifurcated naturally at the tip of the new channel in 2007. The river length decreased abruptly by 16 km and 5 km due to water diversion and natural bifurcation, respectively (Fig. 2C). Dredging was performed along the channel reach downstream of Q8 during 1988–1992, but the impacts were argued to be minor (Wang, 2010). In addition, levees, farm dikes, country roads, short spur dikes and flow diversion projects have been intermittently constructed along the channel (Wang, 2010; Zheng et al., 2017).

The study channel reaches include 21 cross-sections from Lijin (denoted as LJ) to C3 and span a river length of ~100 km (Fig. 2). Because the avulsion location in 1976 was close to HK7 (Fig. 2B), the channel reaches are divided into an upstream reach between Lijin and HK7 and a reach downstream of HK7. It should be noted that surveys at the downstream cross-sections began later than those at the upstream sections (Fig.2).

Water discharge and sediment load at Lijin decreased dramatically immediately following the construction of the Longyangxia and Xiaolangdi Dams in 1986 and 1999, respectively (Fig. 3A, see Fig. 2A for the locations of the dams). The river experienced many days without water discharge at Lijin during 1990–2000 due to low precipitation and excessive water and sediment withdrawals, among other reasons (Wang and Liang, 2000) (Fig. 3B). A minimum water discharge has been maintained at Lijin since 2000 to avoid this situation of no water discharge by implementing a water resource allocation scheme to the eight provinces along the Yellow River. In addition, artificial floods have been created by regulating the water discharge and sediment

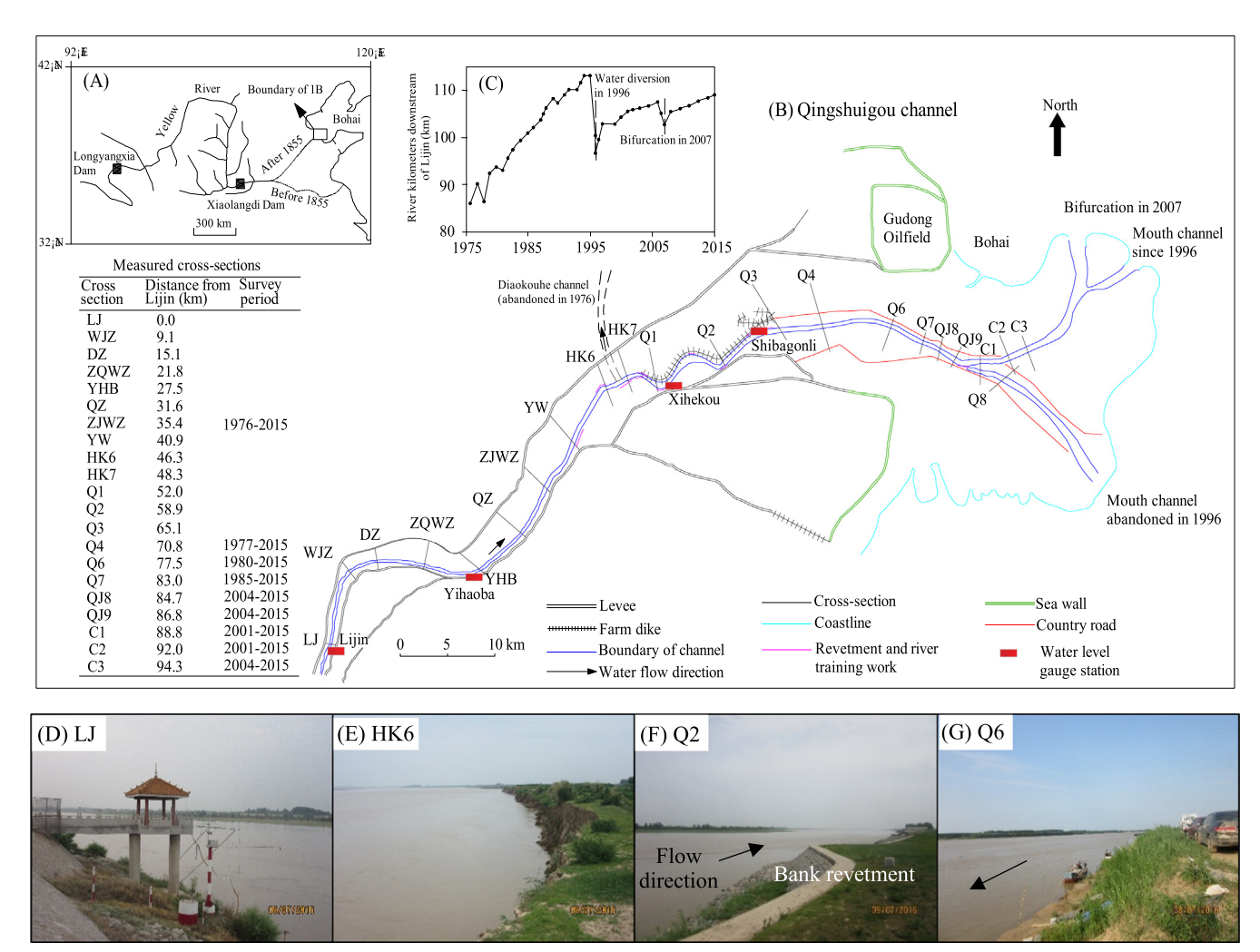


Fig. 2. Study area: (A) Shift of the lower Yellow River in 1855, (B) Qingshuigou channel, (C) changes in river length from Lijin to the shoreline, and channel near the cross-section of (D) LJ, (E) HK6, (F) Q2, and (G) Q6.

Table 1Main disturbances to the Qingshuigou channel.

Disturbance		Time	Location	Main impacts
Alteration to channel boundary (and coastal) conditions	Artificial avulsion	May 1976	Near HK7 (Fig. 2B)	River was diverted to the Qingshuigou channel and the Diaokouhe channel was abandoned (Fig. 2B).
	Water diversion	May-July 1996	Near Q8 cross-section	River flow was diverted to the northeast mouth channel (Fig. 2B).
	Dredging	1988–1992	Channel reaches at the downstream of ~Q8	The impact may be limited at the downstream reach (Wang, 2010).
	Natural bifurcation	2007	At river mouth (Fig. 2B)	New branch started to transport most of the water and sediment load to the sea.
Alteration to water and sediment conditions	Dam construction	Longyangxia Dam in 1986 Xiaolangdi Dam in 1999	At the upper Yellow River (Fig. 2A) ~764 km upstream of Lijin (Fig. 2A)	Water discharge and sediment load transported to the Yellow River delta decreased.
	No water discharge	1990–1999 (most severe period, Fig. 3B)	Lower Yellow River and the delta	There was little water discharge at Lijin and salted water intruded towards upstream.
	Water and sediment regulation	2002-present	By operation the Xiaolangdi and other reservoirs	Artificial floods have been regulated to scour the channel bed of the lower Yellow River.

load via operations at Xiaolangdi Dam and several other reservoirs since 2002. This water and sediment regulation scheme (WSRS) has slightly increased the water discharge at Lijin. However, the sediment load is still low.

3. Data and methods

Table 2 lists the data used in this study, which were measured and provided by the YRCC. Some of the data have been published online or used in existing studies. The flood season for the Yellow River basin is from Jul. to Oct., and the nonflood season is from Nov. to Jun. of the following year. Cross-sectional profiles were generally surveyed twice a year, one time before the flood season and the other by the end of the flood season in Oct. A digital echo sounder, microwave positioning device and GPS system were used in the measurements (Wu et al., 2017). The time periods for the surveys of cross-sections are shown in Fig. 2. Water surface elevation was measured only at Yihaoba, Xihekou and Shibagongli, and there are no data for water surface elevation available downstream of cross-section Q3 (Fig. 2). Measurements at Shibagongli were discontinued after 1990.

The aggradation or degradation volume in the channel reaches was estimated using a method adopted from Kasai et al. (2004) and Zheng et al. (2014, 2018). Following this method, the erosion or deposition volume between two adjacent cross-sections equals the average changes in the cross-sectional areas multiplied by the river length between the two cross-sections. The erosion or deposition volume per river kilometer V (m^3/km) at a channel reach can be calculated by:

$$V = \frac{\sum_{i=1}^{N-1} \frac{1}{2} (\Delta A_i + \Delta A_{i+1}) L_{i,i+1}}{\sum_{i=1}^{N-1} L_{i,i+1}} = \frac{\sum_{i=1}^{N-1} \frac{1}{2} (\Delta A_i + \Delta A_{i+1}) L_{i,i+1}}{L_{1,N}}$$
(1)

where $\Delta A_i = \text{cross-sectional}$ area change of the i^{th} cross-section (m²); $L_{i,\ i+1} = \text{river}$ length between the i^{th} and $(i+1)^{th}$ cross-sections (km); $L_{1,\ N} = \text{river}$ length between the 1st and last (N^{th}) cross-sections (km); and N = number of cross-sections in the channel reach. Eq. (1) was used to estimate the cumulative erosion or deposition volumes per river kilometer in the upstream and downstream reaches by the end of flood season. The upstream reach between LJ and HK7 has a river length of ~48 km, whereas the length of the downstream reach varied in different time periods due to a lack of surveys at some downstream cross-sections (Fig. 2). For example, the river length of the downstream reach was ~17 km between HK7 and Q3 in 1976, ~22 km between HK7 and Q4 from 1977 to 1980, ~29 km between HK7 and Q6 from 1980 to 1985, and ~35 km between HK7 and Q7 from 1985 to 2015.

To calculate the change in cross-sectional area, we selected an arbitrary datum for each cross-section, and this datum is high enough that any changes in the cross-section, including erosion or deposition in the main channel and on the floodplains, are bounded by the datum and the channel boundary. We denote this datum as Datum_XS, as shown in Fig. 4A, which takes Q2 as an example. For each cross-section, the Datum_XS is fixed so that changes in the cross-sectional area below this elevation reflect the erosion or deposition in the whole channel (including the main channel and floodplain). It should be noted that the floodplains are very wide at some cross-sections, especially those in the lower reaches (e.g., Q2 in Fig. 4A), and that subsidence of the floodplain and human activities such as trenching may impact the changes in the cross-sectional areas. Therefore, it is also important to estimate the erosion or deposition volume in the main

To estimate the changes in the cross-sectional area of the main channel, a datum, denoted as Datum_MC, is selected for each cross-section (Fig. 4B). This datum is close to the bankfull elevation and generally lower than Datum_XS. Datum_MC is also fixed for each cross-section during the whole survey time period so that the change in the area bounded by this datum and the channel boundary reflects the general erosion or deposition in the main channel. The width of the main channel is taken as the horizontal distance between the intersection points of this datum and the channel boundary on the left and right banks. The depth of the main channel is the ratio of the cross-sectional area of the main channel to its width. The average channel bed elevation is calculated by subtracting the main channel depth from Datum_MC for each cross-section. Using the average bed elevation at the cross-sections, the channel longitudinal profiles can be plotted and fitted by linear lines. The channel slope is taken as the slope of the linear regression lines of the channel's longitudinal profiles if the coefficient of determination $R^2 > 0.5$ (Zheng et al., 2018).

The channel backwater length (L_b) is estimated as the ratio of the average water depth at Lijin (H) to the average channel bed slope downstream of Lijin (S) (Nittrouer et al., 2012):

$$L_b = H/S \tag{2}$$

where *H* is calculated based on the measurements of water discharge, water surface elevation and cross-sectional profiles at Lijin station.

In this study, we use the normalized superelevation (denoted by NS) and the lateral migration rate of the main channel to estimate channel activity and its tendency for avulsion. The calculation method for NS is adopted from Zheng et al. (2018) and is the ratio of the superelevation of the bank top above the surrounding floodplain to the channel depth from the thalweg to the top of the bank. The normalized lateral migration rate of the main channel (yr $^{-1}$) is the ratio of the average lateral migration rate of the thalweg (m·yr $^{-1}$) to the main channel width (m).

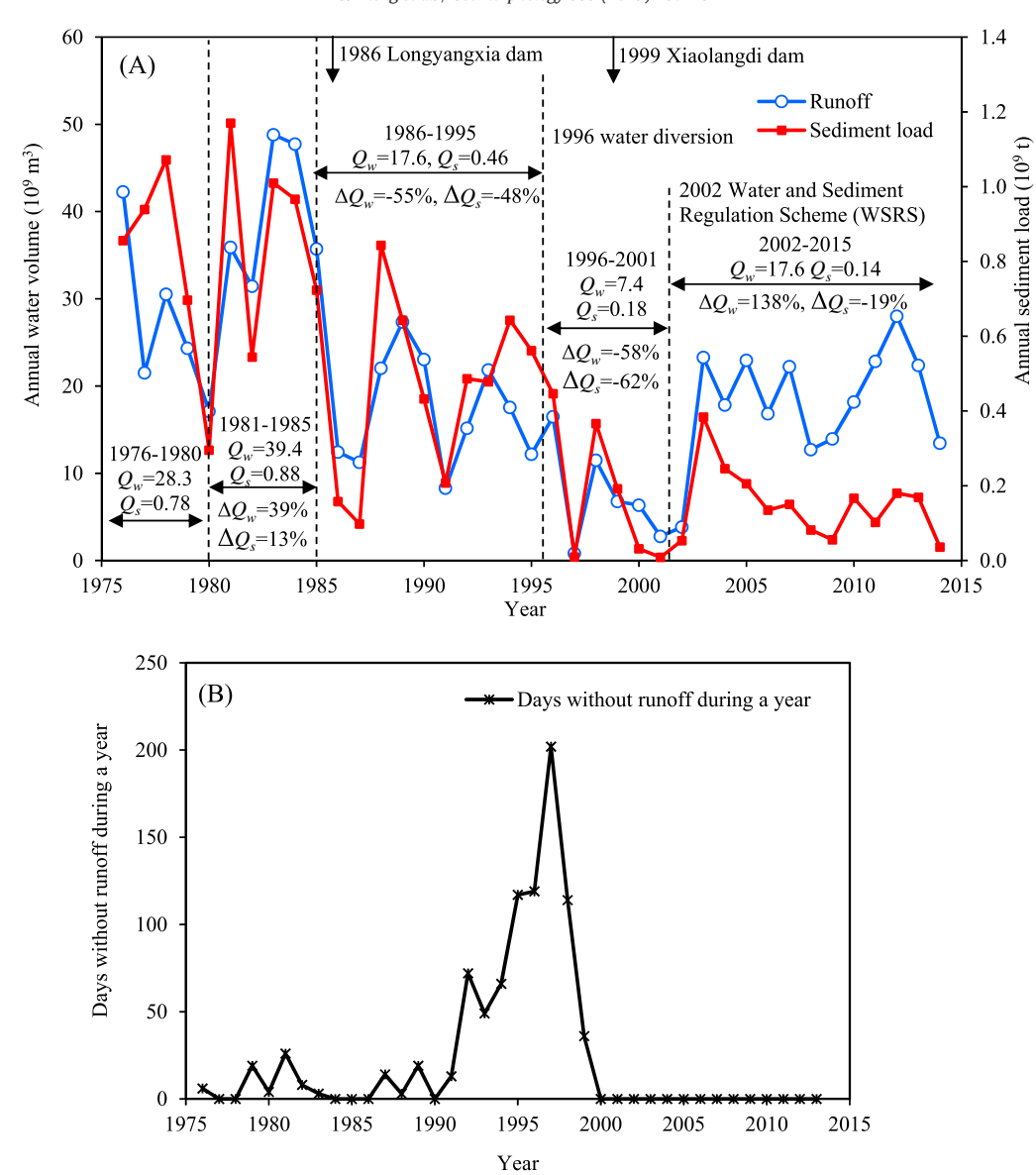


Fig. 3. Water and sediment conditions at Lijin: (A) annual water discharge Q_{sv} (billion m^3) and sediment load Q_s (billion t), and (B) days without water discharge. Note: Lijin gauge station is the last station at the lower Yellow River. ΔQ_{sv} and ΔQ_s (%) = changes in Q_{sv} and Q_s comparing with those in last time period, respectively. Q_{sv} and Q_s decreased dramatically immediate following the construction of the Longyangxia and Xiaolangdi Dams in 1986 and 1999, respectively. Q_{sv} increased but Q_s was still low after the implementation of the water and sediment regulation scheme (WSRS) in 2002.

4. Results

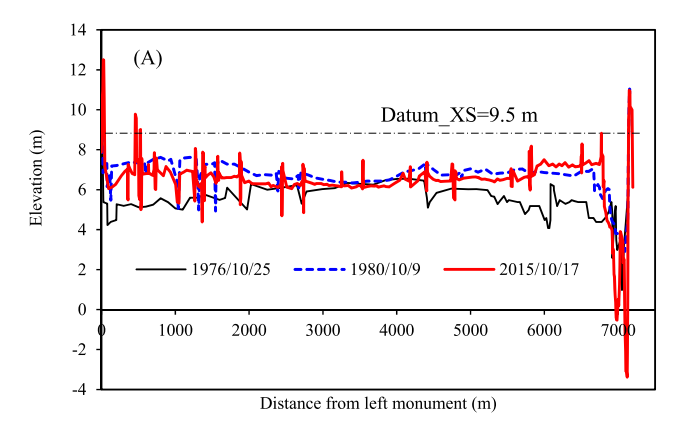
4.1. Deposition and erosion processes in the Qingshuigou channel

From 1976 to 1977 immediately following the avulsion, the upstream reach of the Qingshuigou channel was eroded slightly (the cumulative erosion or deposition volume per river kilometer in the upstream reach V_u was negative in Fig. 5), whereas the downstream reach experienced rapid deposition (V_d in the downstream reach was

positive). Erosion in the upstream reach may be attributed to relatively high flow (Fig. 3A) and the abrupt decrease in elevation as the bed of the excavated Qingshuigou reaches was much lower than that of the abandoned Diaokouhe channel (Wang, 2010). The changes in V_u in the upstream channel reach and V_d in the downstream reach exhibited similar patterns after 1977 and were generally characterized by four phases, i.e., two aggradation phases from 1977–1980 and 1985–1996 and two degradation phases from 1980–1985 and 2002–2015. The channel slightly degraded and then aggraded from 1996–2002,

Table 2List of measurement data used in this study.

Measurement data	Time period	Data published in
Annual water discharge and sediment load at Lijin station	1976-2015	Bi et al. (2014); Zhou et al. (2015); Wu et al. (2017); Zheng et al. (2017, 2018)
Daily water surface elevation at Lijin		=
River length from Lijin to the shoreline	1976-2015 (Fig. 2C)	Zheng et al. (2017, 2018)
Cross-sectional profile	21 cross-sections with different survey time periods (Fig. 2)	Zhang et al. (2005); Wu et al. (2017)



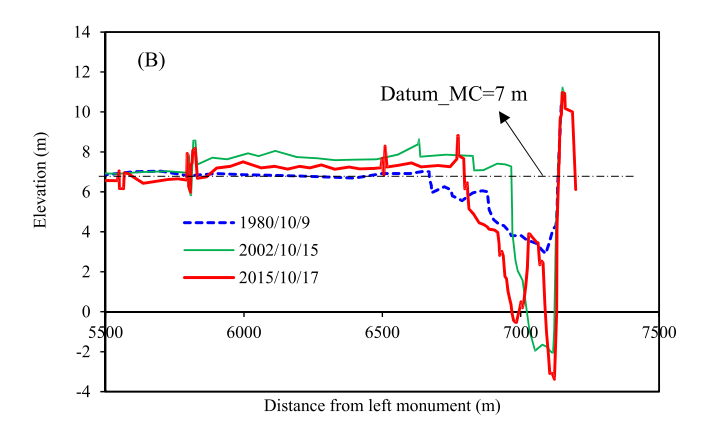


Fig. 4. Selected datum: (A) Datum_XS for estimating the changes in the whole cross-sectional area (including main channel and floodplains), and (B) Datum_MC for estimating changes in the main channel area. Q2 cross-section is taken as an example. Note that Datum_XS should be high enough so that changes in the main channel and the floodplains are bounded by this datum and the cross-sectional profile. Datum_MC is close to bankfull elevation. These two elevations were selected according to the changes in channel geometry and were kept constant during the survey period for each cross-section.

resulting in little change in V_d and V_u . It should be noted that massive sedimentation in the downstream reach from 1976 to 1980 led to much higher values of V_d than V_u . During this time period, the evolution of the downstream channel reaches may have been significantly impacted by the initial channel boundary and floodplain topography as the channel shifted frequently.

From 1980 to 2015, there is an inverse relationship between the volumetric change per river kilometer in Qingshuigou channel V and water discharge Q and a direct relationship between V and the incoming sediment coefficient ξ (Fig. 6). Note that V in Fig. 6 is the sum of V_u and V_d in Fig. 5 and is calculated for the channel reach between LJ and Q6 from 1980 to 1985 and that for between LJ and Q7 thereafter due to a lack of surveys at Q7 before 1985. ξ is defined as the ratio of sediment concentration to water discharge (Wu et al., 2008a), and previous studies have shown that ξ impacts the geomorphologic evolution of the lower Yellow River (e.g., Xu, 2003; Wu et al., 2008a, 2008b). The correlation coefficient (R) between V and Q is -0.66, whereas that between V and ξ equals 0.60, implying that a greater discharge and a lower incoming sediment coefficient cause more erosion and vice versa (Fig. 6).

As expected, changes in the longitudinal profile of the Qingshuigou channel by the end of the flood seasons were closely related to the erosion and deposition processes (Fig. 7). The longitudinal profile upstream of the avulsion point was lowered from 1976 to 1977 due to channel erosion and then raised from 1977 to 1980 due to deposition (Fig. 7A). The longitudinal profile downstream of the avulsion point is not shown in 1976 and 1977 because a single-thread main channel had not formed. The channel bed was eroded from 1980 to 1985, aggraded from 1985 to 1996, and eroded again from approximately 1996 to 2015 (Fig. 7B).

The slope of the downstream channel reach was more than three times greater than that of the upstream reach immediately following the avulsion and decreased rapidly as time elapsed (Fig. 7C). This result is consistent with the argument by Zheng et al. (2017) that the slope of the characteristic water level in the lower Qingshuigou channel decreased exponentially with time following the avulsion in 1976. It should be noted that the thalweg elevation in the downstream reach was used to estimate the channel slopes from 1976 to 1977 before the formation of the main channel. The slopes of the upstream and downstream reaches became approximately equal in the early 1980s, implying that the channel slope had relaxed considerably in response to the abrupt artificial avulsion. Interestingly, the slope of the longitudinal profile of the Datum_MC (close to bankfull elevation) at the cross-sections (0.116%, Fig. 7B) was slightly greater than the average channel bed slope from 1976 to 2015 (0.098%).

4.2. Backwater impacts on the Qingshuigou channel

4.2.1. Backwater length

Because the cross-sectional profile at Lijin was surveyed twice every year, the backwater length could be estimated twice (Fig. 8A). We refer to these two sets of values as the backwater length pre- and post-flood

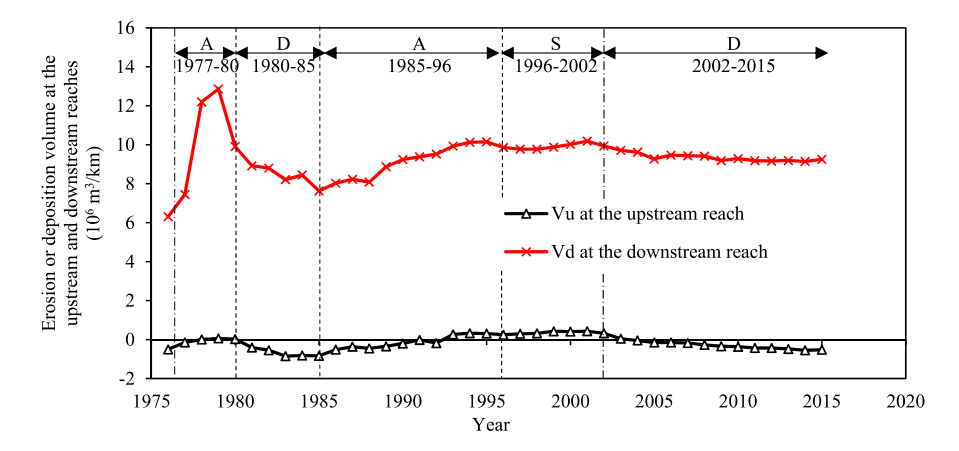
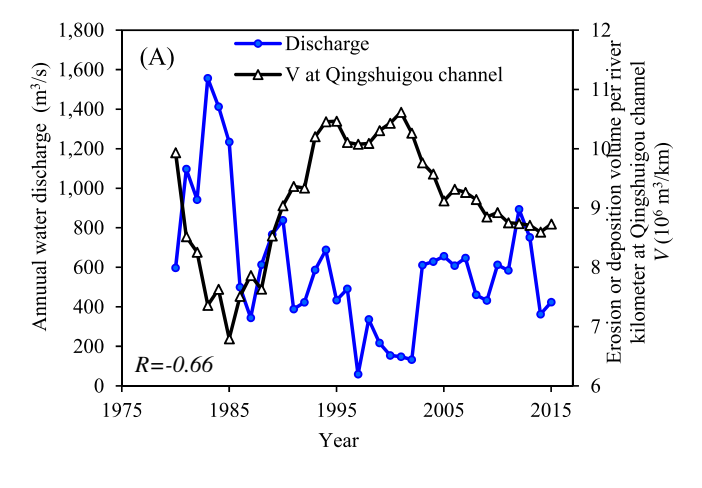


Fig. 5. Cumulative erosion or deposition volume per river kilometer at the upstream reach between LJ and HK7 (V_u) and at the downstream (V_d) by the end of the flood seasons. Note that V_u and V_d include erosion and deposition in the main channel and the floodplains. River length of the upstream reach between LJ and HK7 is ~48 km, whereas that of the downstream reach varied during different time periods due to the lack of surveys at some downstream cross-sections (Fig. 2). The changes in V_u and V_d exhibited a similar pattern after 1977 and were generally characterized by four phases, i.e. two aggradation phases (denoted by 'A') from 1977–1980 and 1985–1996, and two degradation phases (denoted by 'D') from 1980–1985 and 2002–2015. The channel was relatively stable (denoted by 'S') from 1996 to 2002.



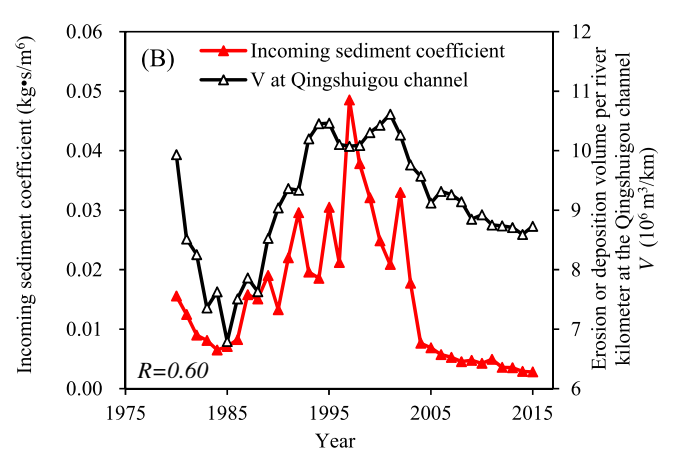
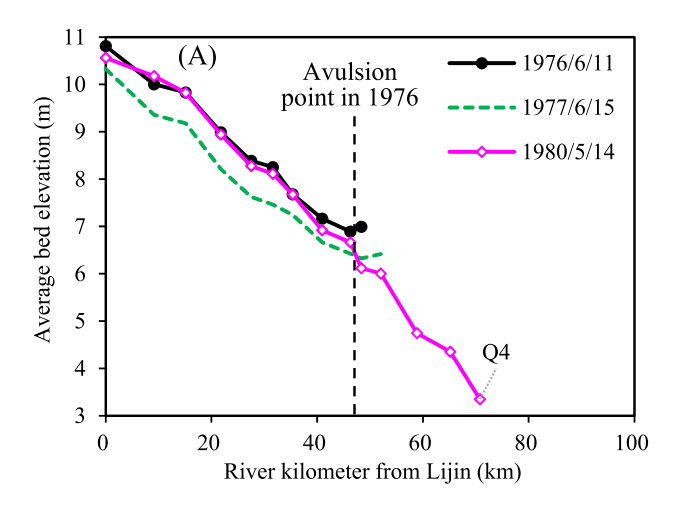
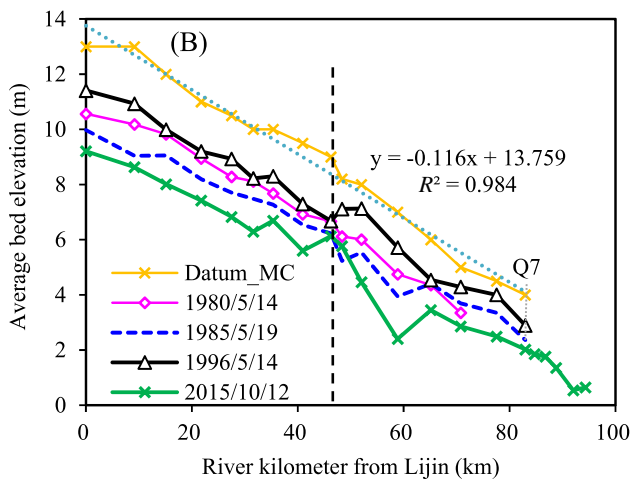


Fig. 6. Relationship between the cumulative erosion or deposition volume per river kilometer at the Qingshuigou channel V from 1980 to 2015 and (A) annual water discharge Q, and (B) incoming sediment coefficient ξ defined as the ratio of sediment concentration to water discharge, respectively. Note that V is the sum of V_u and V_d in Fig. 5, and it was calculated for the channel reach between LJ and Q6 during 1980–1985 and that between LJ and Q7 thereafter due to a lack of surveys at Q7 before 1985.

seasons. The estimation result of backwater length is shown in Fig. 8A. The breaks in the line representing the backwater length pre-flood season in Fig. 8A are due to a lack of data during times of little water discharge at Lijin. Ideally, the backwater lengths would be calculated from data during flood and nonflood seasons since these times are when bed changes occur, rather than during pre- and post-flood seasons. However, the backwater length during flood seasons could not be calculated directly because there is no survey of cross-sectional profiles during flood seasons. Since the backwater length was closely related to water discharge Q, and the value of Q during flood seasons from 1976 to 2015 (23–3071 m³/s with a mean value of 1162 m³/s) was similar to that at the end of flood seasons in Fig. 8B $(76-3860 \text{ m}^3/\text{s})$ with an average of 1163 m³/s), the average backwater length during flood seasons may be close to that of the post-flood season. The pre-flood season Q varied from 0 to 1060 m³/s with an average value of 204 m³/s (Fig. 8B), whereas during nonflood seasons, the value varied from 41 to 781 m³/s with an average of 364 m³/s. Thus, the average backwater length during nonflood seasons may be slightly longer than that during pre-flood seasons.

The backwater lengths post-flood seasons varied from 7 to 53 km with an average of 22 km and were generally longer than those for pre-flood seasons, which varied from 2 to 25 km with an average of 14 km (Fig. 8A). The greater backwater lengths post-flood seasons were due to greater water discharge, although the channel slopes pre-and post-flood seasons did not differ much (Fig. 8B–C). However, the channel slope after flood seasons was slightly less than that before





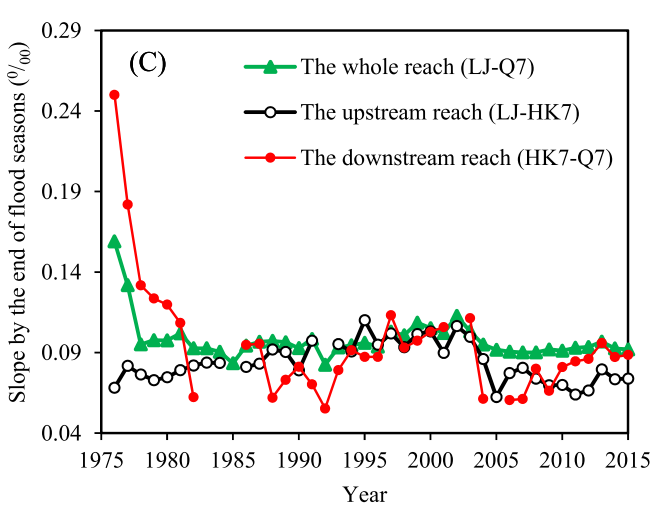


Fig. 7. Channel long profile from (A) 1976–1980, (B) 1980–2015, and (C) temporal changes in longitudinal slope of the upstream, downstream and whole channel reaches by the end of flood seasons. It should be noted that the thalweg elevation at the downstream reach was used to estimate the channel slopes from 1976 to 1977 before the formation of the main channel. The slope at the downstream channel reaches was more than three times greater than that at the upstream reach immediately following the artificial avulsion in 1976, and it decreased rapidly as time elapsed. In the early 1980s, the upstream and downstream slopes became in-phase implying that the channel slope had almost relaxed in response to the abrupt avulsion. Datum_MC represents datum selected for estimating main channel changes (Fig. 4B).

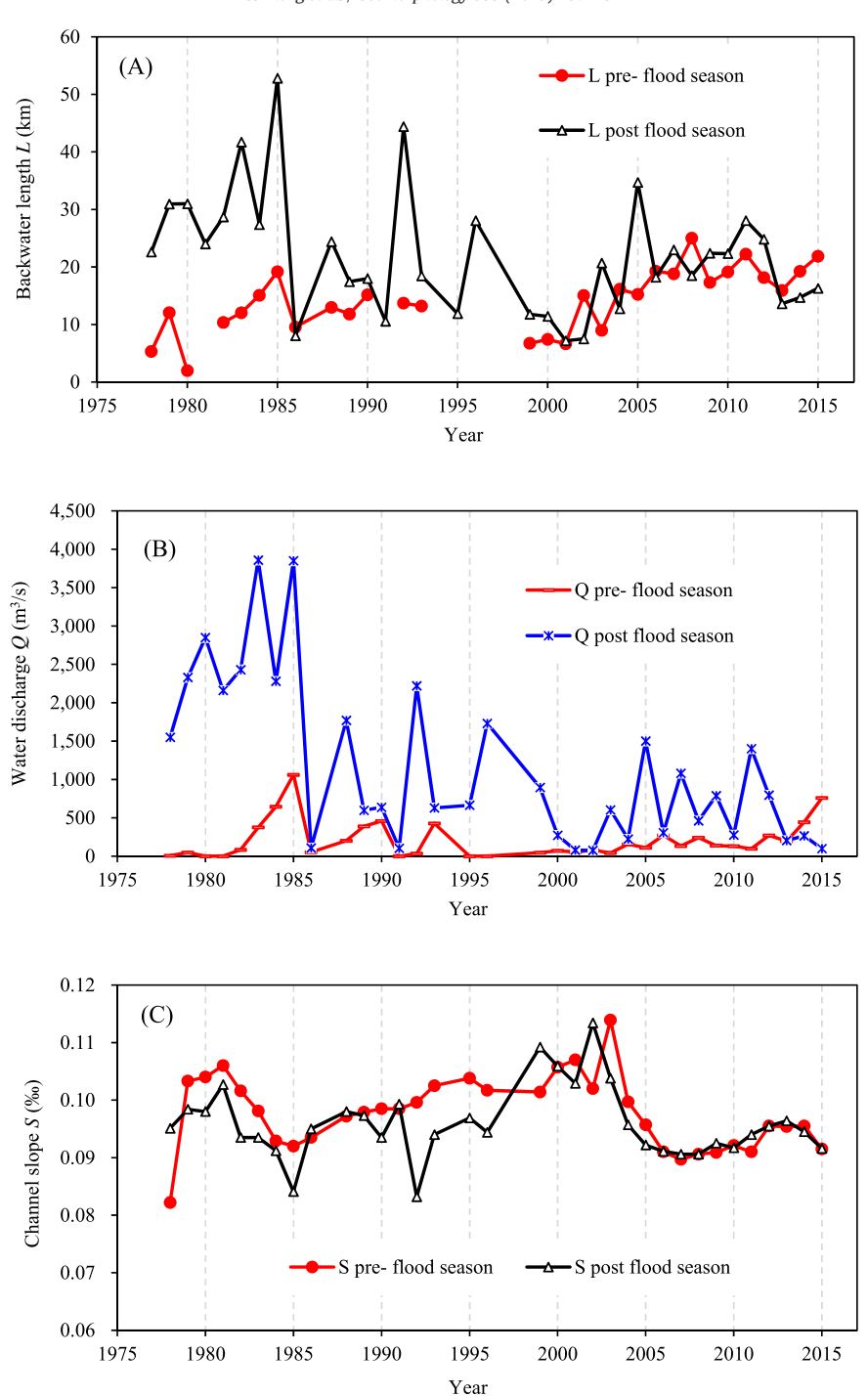


Fig. 8. (A) Backwater length, (B) daily water discharge on days when Lijin cross-section was surveyed, and (C) channel slope pre- and post- flood seasons at the Qingshuigou channel. The breaks in the line representing backwater length pre-flood seasons in Fig. 8A are due to no data since there was little water discharge at Lijin.

flood seasons presumably due to degradation during flood seasons (Fig. 8C). We calculated a correlation coefficient of R=0.73 between the water discharge and backwater length using all the data (pre- and post-flood seasons).

Interestingly, the backwater lengths pre- and post-flood seasons were similar after approximately 2000 (Fig. 8A), although the water discharges for post-flood seasons were greater than those for pre-flood seasons (Fig. 8B). This difference may have occurred because after the implementation of the WSRS in 2002, the channel bed was incised significantly (Fig. 7B) and became relatively narrow and deep (Zheng et al., 2018, Fig. 10B). Therefore, the backwater length after ~2002 may be longer than those in previous time periods under the same discharge.

4.2.2. Hydrodynamic backwater effects

In this sub-section, we compare the spatial distribution of the erosion and deposition volume along the Qingshuigou channel with that expected under hydrodynamic backwater effects. Hydrodynamic backwater effects create a zone of enhanced in-channel sedimentation because of spatial deceleration and deposition during low flows and spatial acceleration and erosion during high flows. We assume that the flows during flood and nonflood seasons are representative of high and low flows, respectively. We calculate the changes in cross-sectional areas of the main channel in flood and nonflood seasons and water years during different time periods (Fig. 9, negative values indicate degradation and positive values indicate aggradation). These time periods are selected according

to the four evolution phases proposed by Zheng et al. (2018). The time period from 1976 to 1980 is not considered herein because it is difficult to identify the main channel in the downstream reach before ~1980. The distance from a cross-section to the shoreline in Fig. 9 is obtained using the average river length from Lijin to the shoreline minus the distance from Lijin to the cross-section (Fig. 2).

The main channel of Qingshuigou generally degraded during flood seasons and aggraded during nonflood seasons (Fig. 9). Maximum sedimentation generally occurred near Q1 or Q2 (~40–60 km upstream of the shoreline) during nonflood seasons. This maximum sedimentation zone was located upstream of the backwater zone since we estimated in the last section that the backwater length during the nonflood season may be slightly greater than that during the pre-flood season, which varied between 2 and 25 km with an average of 14 km. Thus, hydrodynamic backwater effects may not be the reason for the maximum sedimentation near Q1 and Q2.

The maximum backwater length was estimated as ~50 km, and the upstream boundary of the backwater zone may extend to Q1 or Q2 during flood seasons (Fig. 8A). The channel was eroded in the lower reach during flood seasons; the erosion rates decreased downstream of Q1 and reached approximately zero at the farthest downstream reach near Q6 or Q7 (Fig. 9). This situation is contrary to the topographic evolution under standard hydrodynamic backwater conditions where drawdown at high flows creates increasing erosion downstream (Chatanantavet et al., 2012; Lamb et al., 2012; Ganti et al., 2016).

The lower channel reaches tended to become wider and shallower from upstream to downstream, and the width to depth ratio (W/H) generally doubled from Q2 to Q7 (Fig. 10B). There is a positive correlation between W/H and changes in the average bed elevation (ΔZ) from Q1 to Q7 during flood seasons in different time periods (Fig. 11). This result indicates that with the increase in W/H from upstream to downstream reaches, the erosion rate decreased along the channel during flood seasons.

4.2.3. Morphodynamic backwater effects

Aggradation and backfilling occur under morphodynamic backwater effects. To analyze the morphodynamic backwater effects, we focus on the second aggradation phase in the Qingshuigou channel from 1986 to 1995 (Zheng et al., 2018).

Sediment deposition from 1986 to 1995 may have been caused by not only the significant decrease in water discharge but also by morphodynamic backwater effects. The average water discharge and sediment load from 1986 to 1995 decreased by 55% and 48%, respectively, compared to values from 1981 to 1985 (Fig. 3A). As shown in Fig. 12A, the changes in cross-sectional areas did not differ much among the cross-sections from 1986 to 1987. As time elapsed, more sediment accumulated in the downstream channel reach than in the upstream reach, consistent with channel backfilling processes under morphodynamic backwater effects (Edmonds et al., 2009; Hoyal and Sheets, 2009).

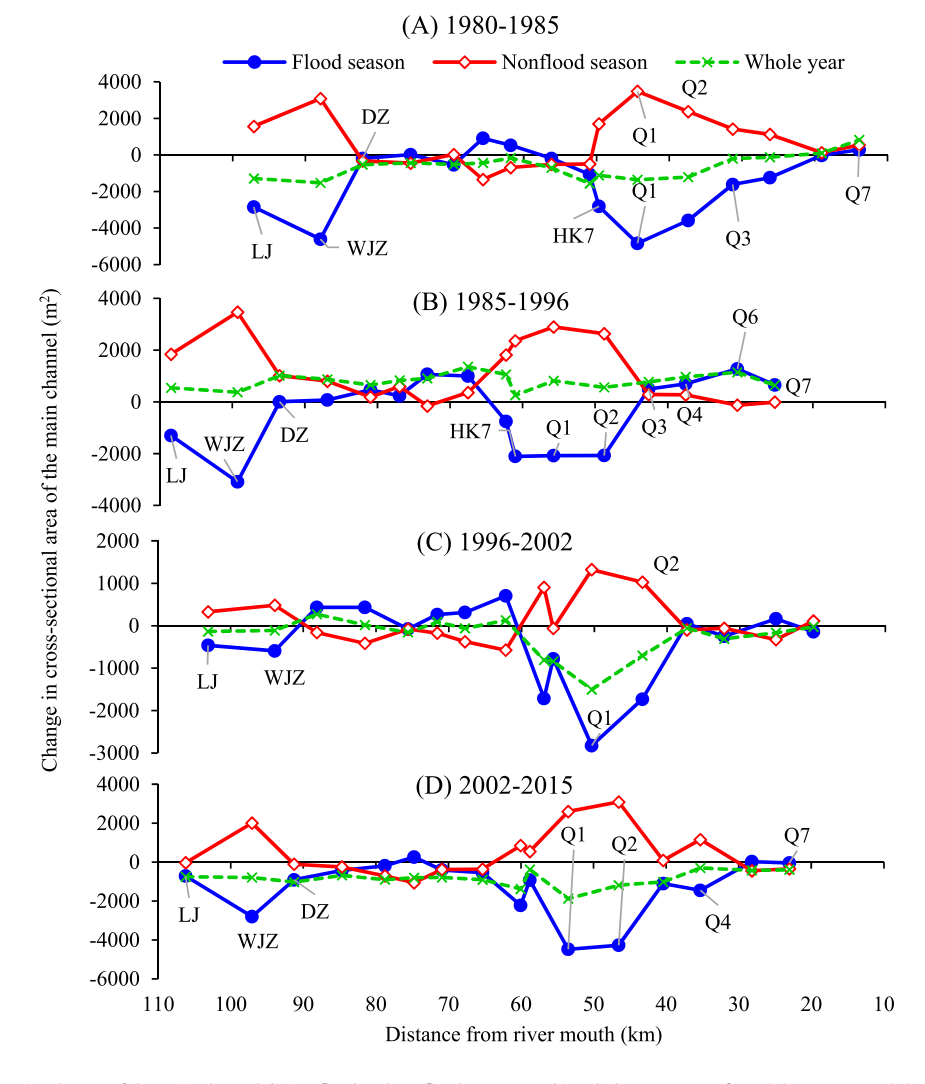


Fig. 9. Total changes in cross-sectional areas of the main channel during flood and nonflood seasons and in whole water years from (A) 1980–1985, (B) 1985–1996, (C) 1996–2002, and (D) 2002–2015. Note the channel was generally eroded during flood seasons and aggraded during nonflood seasons.

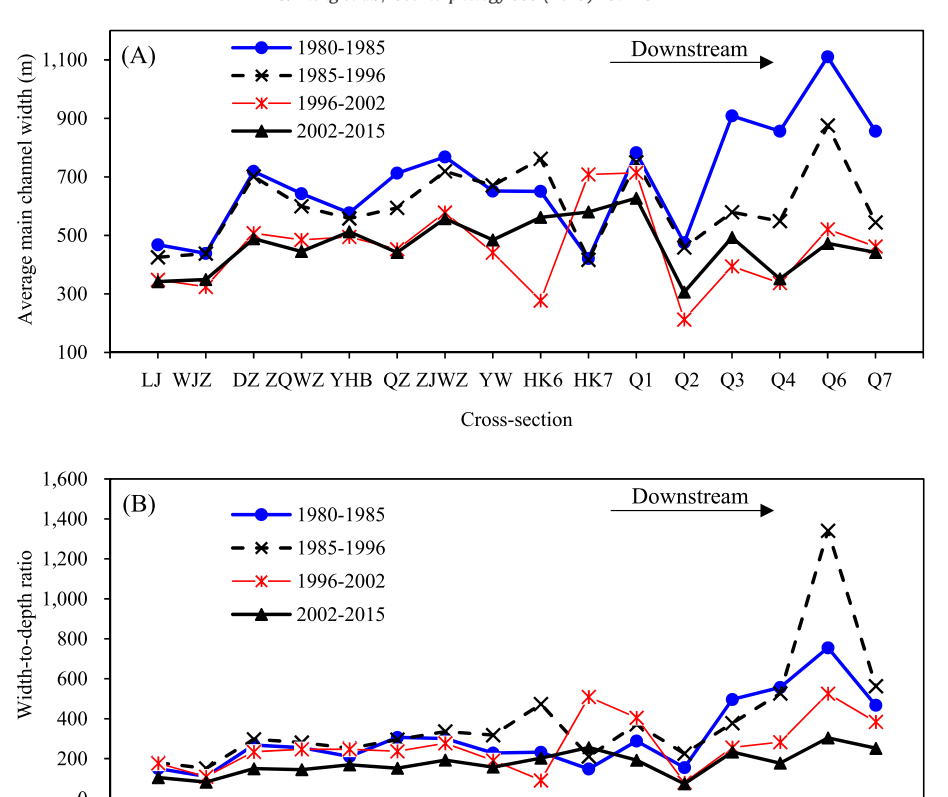


Fig. 10. Changes in (A) main channel width, and (B) width-to-depth ratio at the cross-sections. The main channel tends to become wide and shallow in the downstream direction between Q1 and Q7.

Cross-section

WJZ DZ ZQWZ YHB QZ ZJWZ YW HK6 HK7 Q1

The values of *NS* at the cross-sections of the lower Qingshuigou channel fluctuated with time, and they were commonly greater at the downstream cross-sections than at the upstream ones (Fig. 12B). *NS* at Q6 and Q7 exceeded the critical value of 1.0 in the early 1990s, indicating a strong tendency for avulsion. After ~1996, however, *NS* at the cross-sections decreased due to channel erosion. The average value of *NS* at the cross-sections from 1986 to 1996 increased in the downstream direction along the lower Qingshuigou channel and reached a peak near Q6 (Fig. 12C).

The superelevation of the channel bed was accompanied by lateral activity, and we calculated R=0.63 between the average values of NS and the normalized lateral migration rates at the cross-sections during this time period (Fig. 12C). The average lateral migration rate at Q6 was almost 0.9 times the main channel width from 1986 to 1996, indicating that the channel near Q6 was unstable. As argued by Zheng et al. (2018), avulsion was prevented in the lower Qingshuigou channel due to strong human interventions, including water and sediment regulation by operating dams and construction of levees and farm dikes.

In addition, bank height increased along the lower Qingshuigou channel from 1985 to 1996, and this change increased in the downstream direction between Q4 and Q7 (Fig. 13A). For example, the average increase in the left and right bank heights at Q1 from 1985 to 1996 was 0.5 m, whereas those at Q6 and Q7 were 1.09 and 1.43 m, respectively. Because there are no protected farms downstream of Q4 (personal communication with Kairong Wang in 2018) and the channel reach is fully alluvial and not constricted by levees, the increase in bank height is probably due to sediment deposition. The bed and bank aggradation and channel superelevation are consistent with the evolution characteristics under morphodynamic backwater effects, as shown in Fig. 1A, where Ganti et al. (2016) argued that morphodynamic backwater effects caused channel bed and banks to aggrade, resulting in channel superelevation and avulsion.

5. Discussion

Q2 Q3 Q4

We observed erosional and depositional patterns in the Oingshuigou channel that were inconsistent with hydrodynamic backwater effect. During the flood seasons (which we consider as high flows), erosion occurred in the backwater zone, and the erosion rate decreased to zero at the most downstream cross-sections (e.g., Q6 and Q7) (Fig. 9). Although hydrodynamic backwater effects can cause erosion in the backwater zone (e.g., Chatanantavet et al., 2012; Lamb et al., 2012), the downstream decrease in erosion rates is contrary to the downstream increase in erosion when drawdown occurred at high flows under hydrodynamic backwater conditions (Chatanantavet et al., 2012; Lamb et al., 2012; Nittrouer et al., 2012; Ganti et al., 2016). Admittedly, the data we used span the flood season, and erosion from drawdown lasts a shorter time, making it difficult to isolate the signal. More likely, though, the downstream widening channel geometry between Q1 and Q7 (Fig. 10) and the subsequent downstream decrease in sediment transport capacity may play a significant role in causing downstream decrease in erosion during flood seasons.

O6 O7

The maximum sedimentation zone during nonflood seasons (near Q1 or Q2) may be located upstream of the backwater zone, which is inconsistent with the dynamics of the hydrodynamic backwater. The sedimentation maximum might be caused by local topography near Q1 and Q2, including meandering bends and constriction from dikes (Fig. 2B), or channel migration at the meanders may facilitate deposition, as argued by Wang and Xu (2018a). Recently, Wang et al. (2018) calculated the channel roughness along the Qingshuigou channel and showed that it was greater at WJZ, Q1, and Q2 than at other transects, and they attributed this difference to the impacts of meandering topography. Greater channel roughness at these bends tended to cause more sediment deposition during nonflood seasons. The sediment deposited during nonflood seasons was transported during flood seasons, resulting in

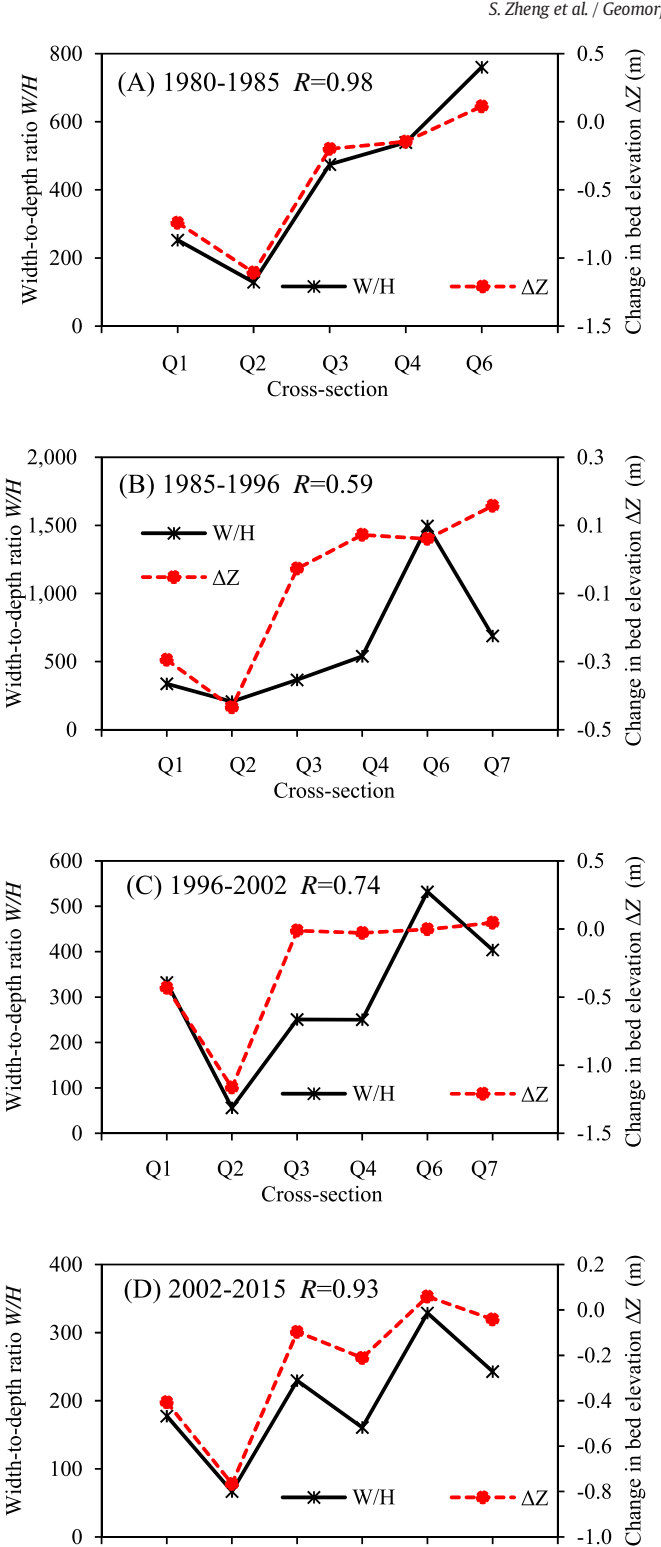


Fig. 11. Correlation between changes in average bed elevation (ΔZ) during flood season and width-to-depth ratio (W/H) in time periods from (A) 1980–1985, (B) 1985–1996, (C) 1996–2002, and (D) 2002–2015. Positive values in ΔZ indicate aggradation and negative values represent degradation. Correlation coefficient $R=0.98,\,0.59,\,0.74$ and 0.93 between W/H and ΔZ for the four time periods, respectively.

Cross-section

Q3

Q4

0

Q1

Q2

\(\bar{Z}\)

Q7

Q6

-1.0

more erosion at these meandering bends during flood seasons (Fig. 9). In addition, farm dikes or levees near Q1 or Q2 may contribute to channel aggradation. Recent studies have recognized sediment deposition within the void space of in-channel dikes and aggradation of point bars due to the construction of dikes (Alexander et al., 2012; Wang and Xu, 2018b). As shown in Figs. 2F, 4 and 13B, the main flow at Q2 was always close to its right bank, which was protected by a revetment, and the left bank and floodplain continued to aggrade from 1976 to 2015. The mechanics of sedimentation near Q1 and Q2 during nonflood seasons need to be further investigated in future studies based on detailed measurements of flow dynamics, sediment transport and bed evolution.

The behavior of the Qingshuigou channel is not consistent with a river forced by the hydrodynamic backwater effects, and this difference suggests that downstream widening of the lower channel reach, meandering, and constriction from dikes may be important factors governing avulsion dynamics. Here, we compare the downstream changes in the channel of the Qingshuigou and the lower Mississippi River (LMR) to further investigate the hydrodynamic backwater effects in deltaic channels with different geometries (Table 3). Although both the Mississippi River Delta and the YRD are fluvial-dominated, the backwater length of the LMR may reach ~500 km and is nearly an order of magnitude greater than that of the Qingshuigou channel due to a greater water depth and gentler slope (Table 3). The width-to-depth ratio W/H of the LMR, calculated using the data in Nittrouer et al. (2012), is considerably less than that of the Qingshuigou channel (Fig. 14). Importantly, W/H decreases downstream during high and low flows along the downstream ~500-km-long backwater-influenced reach of the LMR, and the decrease in W/H is greater during high flows. This trend of downstream decreasing W/H may enhance flow acceleration and amplify erosion and drawdown in the backwater zone of the LMR during high flows. Drawdown caused by hydrodynamic backwater effects during high flows may be more likely to occur in relatively narrow and deep deltaic channels with gentler slopes, e.g., the LMR, rather than in the steep, downstream widening lower reach of the Qingshuigou channel (Fig. 11).

In addition, sediment properties may result in different backwater effects in the LMR and the Qingshuigou channel. As argued by Edmonds and Slingerland (2010), sediment cohesion exerts an important control on delta network formation by stabilizing levees, river mouth bars and bifurcations. The proportion of cohesive silt and clay relative to non-cohesive sand in the Mississippi River is approximately four times greater than that in the Yellow River (Edmonds and Slingerland, 2010). In light of this contrast, the morphodynamic backwater caused by deposition and gradual stabilization of the mouth bar of the LMR may have a greater impact than that of the YRD. However, as argued by Ganti et al. (2016), the upstream migrating wave of deposition caused by morphodynamic backwater is unlikely to persist in natural, low-gradient deltaic systems (such as the LMR) with backwater hydrodynamics because erosion preferentially occurs within the downstream portion of the backwater zone during high flood discharges. Therefore, morphodynamic backwater effects may cause channel bifurcation rather than lobe avulsion at the LMR.

We observed evidence for morphodynamic backwater effects in the lower Qingshuigou channel in the late 1980s and early 1990s. Aggradation rate, bank accretion, superelevation and lateral migration rates of the main channel all tended to increase downstream during the period from 1986 to 1996 (Figs. 12-13). In addition, previous studies have argued that channel aggradation and backfilling from morphodynamic backwater are often accompanied by gradual progradation of a mouth bar (Hoyal and Sheets, 2009, Edmonds et al., 2009). Fig. 15 adopted from Zeng et al. (1997) shows that the mouth bar at the Yellow River estuary migrated seaward rapidly from 1984 to 1987, and the migration rate slowed from 1987 to 1992. Based on bathymetric survey data, Wu et al. (2017) argued that the land area in the active Yellow River Delta lobe accreted slowly from 1982 to 1996. These studies imply sedimentation and gradual progradation of the mouth bar at the lower Oingshuigou channel in the late 1980s and early 1990s, thus providing support for the morphodynamic backwater effects.

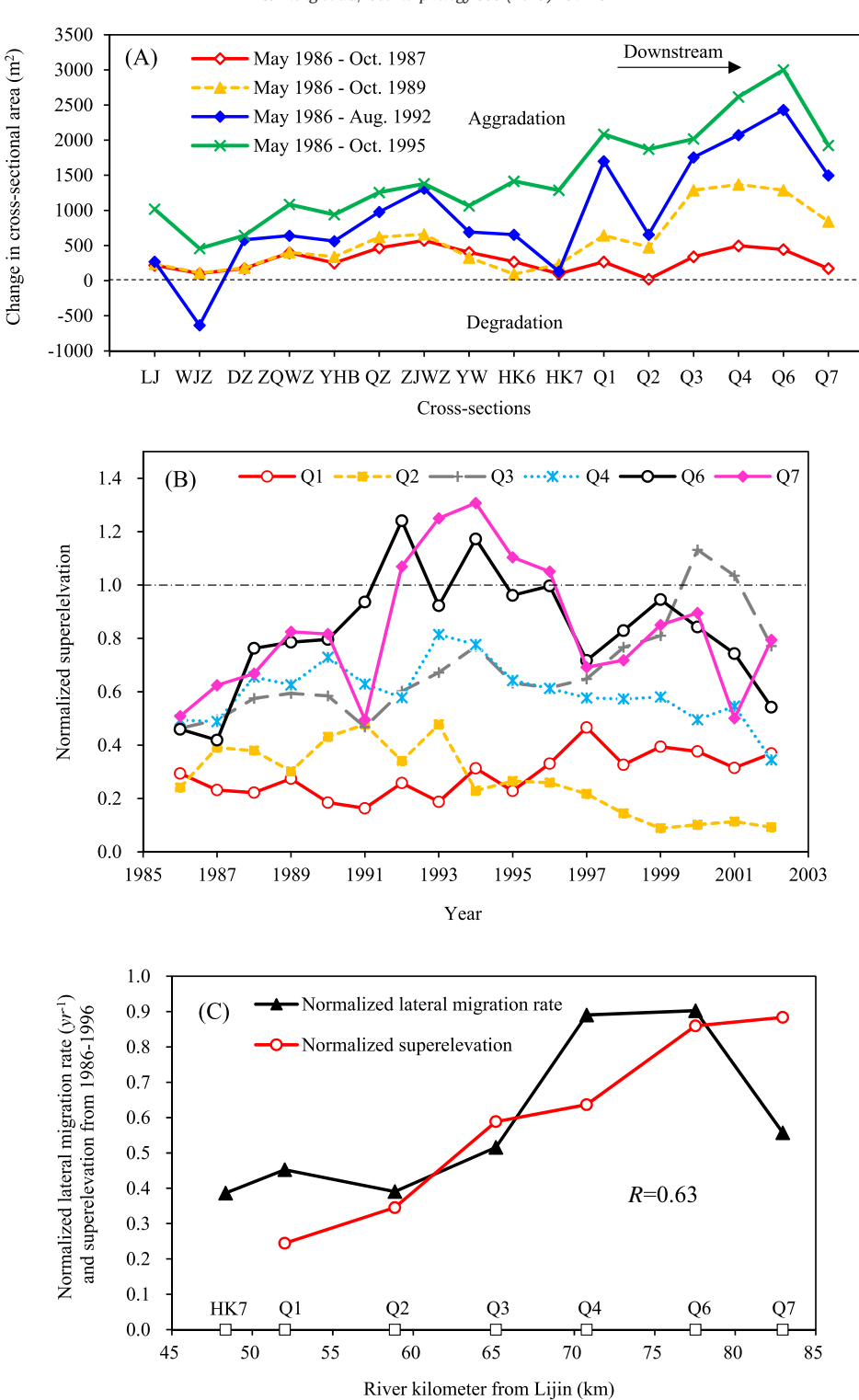
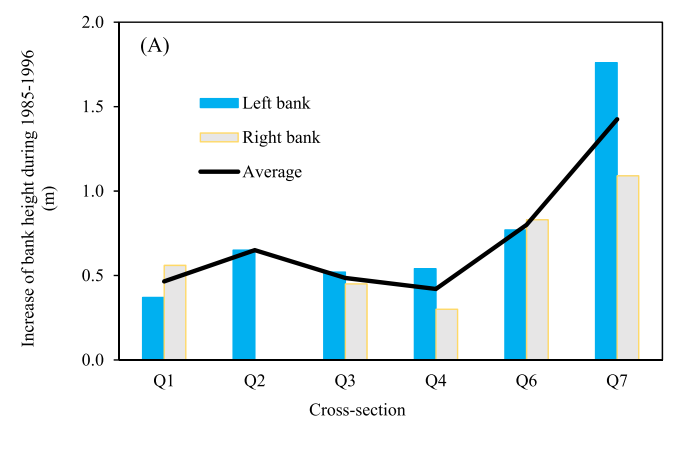
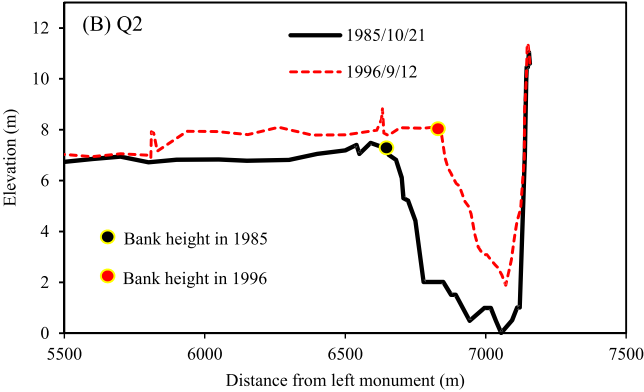


Fig. 12. Sedimentation at the lower Qingshuigou channel: (A) changes in whole cross-sectional areas from 1986 to 1995, (B) normalized superelevation (NS), and (B) correlation between the average values of normalized lateral migration (yr^{-1}) and NS at lower cross-sections from 1986 to 1996. Note NS is calculated using the method in Zheng et al. (2018) and is the ratio of superelevation of bank tops above surrounding floodplain (m) to channel depth (m). Normalized lateral migration (yr^{-1}) is the ratio of average lateral migration rate of thalweg ($m \cdot yr^{-1}$) to the main channel width (m). Deposition volume, superelevation and lateral migration rates generally increased in the downstream direction between Q1 and Q7 from 1986 to 1996.

The calculated results of NS and lateral migration rates in the early 1990s indicated that the channel was most prone to avulsion near Q6 or Q7. Thus, the most likely avulsion length (streamwise distance from the avulsion node to the shoreline) may be estimated as ~20–30 km upstream from the shoreline. Interestingly, this avulsion length is close to those estimated by previous studies. For example, Ganti et al. (2014) computed an average avulsion length of 31.1 km

with a scatter between 24.5 and 48.3 km for seven natural avulsions that occurred on the YRD between 1889 and 1930, based on Pang and Si (1979) and Chu et al. (2006). The similar avulsion lengths may support the argument by Ganti et al. (2014) that avulsions on the YRD may be backwater-mediated. On the other hand, since the channel superelevation near Q6 and Q7 was primarily caused by aggradation under morphodynamic backwater effects, this result indicates that





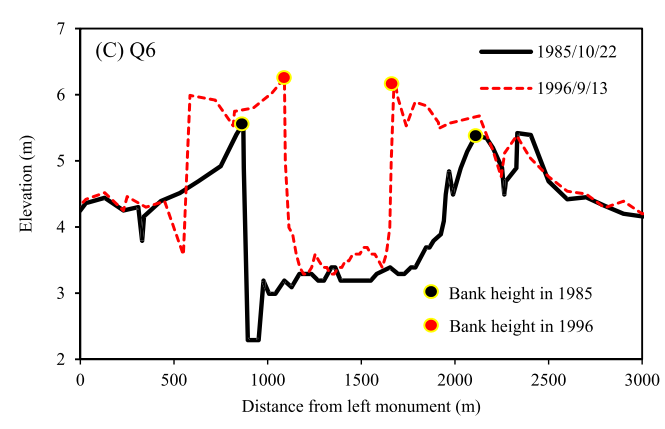


Fig. 13. (A) Increase of bank height from 1985 to 1996, and examples at (B) Q2 and (C) Q6. Note that the right bank at Q2 was protected by revetment (Fig. 2F), thus the increase of the right bank height was not considered.

morphodynamic backwater effects may play a more important role than hydrodynamic backwater in leading up to avulsion in the Qingshuigou channel. Because there are no surveys of channel topography downstream of Q7 from 1985 to 1996, we could not investigate the evolution of the most downstream 20–30-km-long channel reach upstream of the shoreline. Detailed measurements of hydrodynamic conditions and channel adjustment are needed, especially along the most downstream reach, to further investigate the hydrodynamic and morphodynamic backwater effects at the Qingshuigou channel in future studies.

It should be noted that the hydrodynamic and morphodynamic backwater effects changed with time as the channel geometry and boundaries evolved. The Qingshuigou channel has been incised and has become narrower and deeper since the implementation of WSRS in 2002. The backwater length increased with the increase in the width-to-depth ratio for the same water discharge (Fig. 8), implying increased impacts of hydrodynamic backwater from 2002 to 2015, Meanwhile, the channel extended seaward at slower rates after the artificial water diversion in 1996 (Zheng et al., 2017; Fig. 1C) due to the dramatic decrease in sediment load (from ~0.46 billion t during 1986-1995 to <0.2 billion t after 1996; Fig. 3A). The new mouth bar scarcely prograded basinward as it did in the late 1980s and early 1990s (Fig. 15), although recent studies have shown that the slope of the subaqueous delta increased due to the deposition of coarser sediment in the nearshore area after the implementation of the WSRS (Bi et al., 2014; Wu et al., 2017). The NS values at the cross-sections between Q1 and Q7 were generally smaller than 1.0 after ~2000, indicating that the channel was no longer superelevated and became relatively stable (Fig. 12B). Morphodynamic backwater effects may have been less profound from 2002 to 2015.

6. Conclusions

In this study, hydrodynamic and morphodynamic backwater impacts in the Qingshuigou channel on the Yellow River Delta were investigated using data from systematically surveys of water discharge, sediment load, cross-sectional profiles and water surface elevation from 1976 to 2015. Flows during flood and nonflood seasons were taken as representative of high and low flows, respectively. Erosion occurred in the backwater zone during flood seasons, and erosion rates gradually decreased to ~zero in the downstream direction in the lower channel reach. Downstream widening channel geometry may have weakened the hydrodynamic backwater effects and caused the downstream decreases in the sediment transport capacity and the erosion rates. Drawdown caused by hydrodynamic backwater effects was absent in the lower Qingshuigou channel during flood seasons and may be more likely to occur in relatively narrow and deep deltaic channels with gentle slopes, e.g., the lower Mississippi River. During nonflood

Table 3Comparison of characteristics of the Yellow and Mississippi River deltas.

Variable	Yellow River Delta	Mississippi River Delta
Delta area (km²)	5400 (Zheng et al., 2017)	~30,000 (Coleman et al., 1998)
Delta type	Fluvial dominated (Wang and Liang, 2000)	Fluvial dominated ^a
Tide	Length of tidal limit <20 km, tide range ~1.1–1.5 m	Tide range ~ 0.4 m ^a
	(Wang and Liang, 2000; Wang, 2010; Zheng et al., 2018)	•
Avulsion time scale	~10 years (Wang and Liang, 2000)	~1500 years (Coleman, 1988)
Average discharge (m ³ /s)	638 ^b	15,452 ^a
Suspended load (kg/s)	12,612 ^b	12,614 ^a
Sediment concentration (kg/m ³)	19.8 ^b	1.11 ^a
Water depth (m)	0–4.4 m ^b	~10-30 (Nittrouer et al., 2012)
Slope	$\sim 9 \times 10^{-5}$ (Fig. 6C)	2×10^{-5a}
Backwater length (km)	~20-50 (Ganti et al., 2016); ~2-53 (Fig. 7A)	~500 (Chatanantavet et al., 201

Note: Water depth at Lijin was calculated on days when the cross-section was surveyed, and water depth =0 corresponds to little water discharge at Lijin.

^a Data after Syvitski and Saito (2007).

^b Values at Lijin based on data from 1976 to 2015.

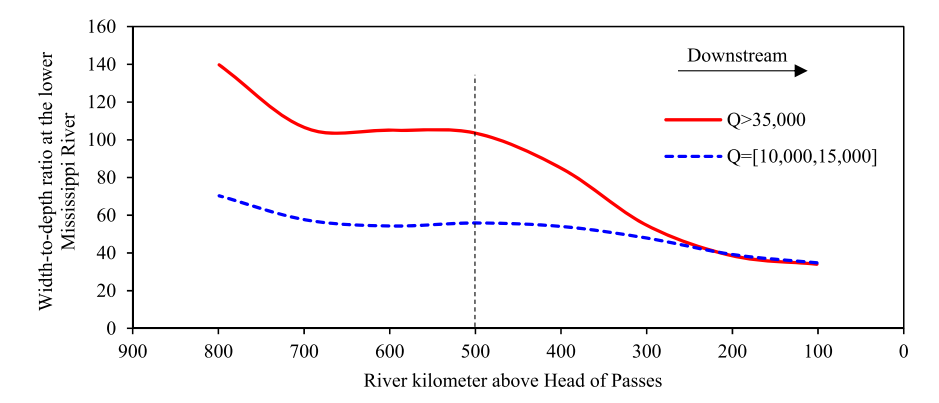


Fig. 14. Width-to-depth ratio at the lower Mississippi River calculated using the data published in Nittrouer et al. (2012). Note there is an obvious downstream decreasing trend of *W/H* at both high and low flows along the downstream ~500-km-long channel reaches, which are influenced by hydrodynamic backwater effects.

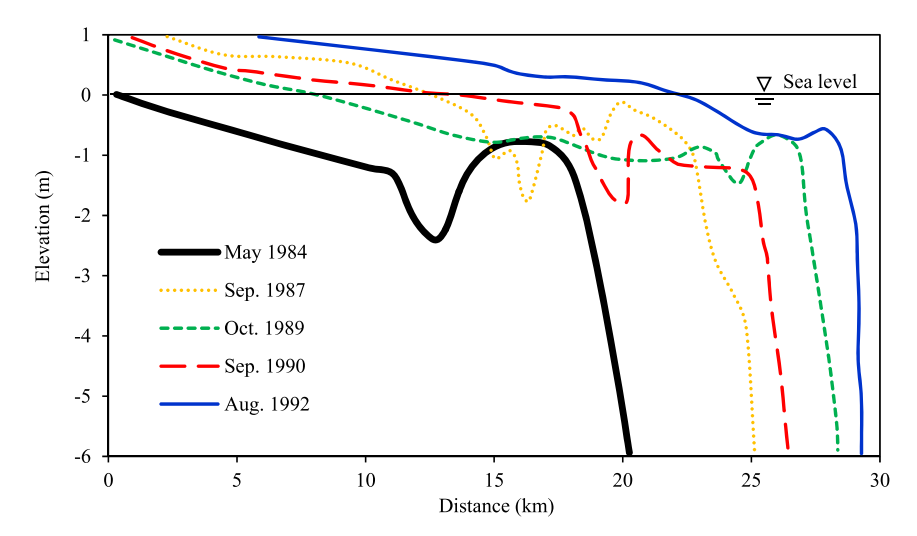


Fig. 15. Longitudinal profile of the lowest channel reach of the Qingshuigou channel, showing gradual progradation of the mouth bar from 1984 to 1992. (After Zeng et al., 1997.)

seasons, maximum sedimentation tended to occur upstream of the backwater zone, presumably due to meandering topography, the construction of farm dikes, etc. These results may imply the impacts of channel geometry on hydrodynamic backwater in the Qingshuigou channel.

Morphodynamic backwater effects, along with the decrease in water discharge, may have caused sediment deposition in the lower Qingshuigou channel from 1985 to 1996. Aggradation rates, channel superelevation and lateral mobility noticeably increased downstream along the lower channel reach. The most likely avulsion location (near Q6 and Q7) was ~20–30 km upstream of the shoreline, a distance that is consistent with the avulsion lengths for historical natural avulsions. These results support the argument that avulsions at the Yellow River Delta may be backwater-mediated and highlight the significant role played by morphodynamic backwater rather than hydrodynamic backwater effects in rendering the channel unstable and susceptible to avulsion.

Acknowledgements

We appreciate the Editor, Professor Zhouyuan Chen, and three anonymous reviewers for their constructive comments, which significantly improved the quality of the original manuscript. This study was funded by the National Key Research and Development Program of China (2017YFC0405202) and National Natural Science Foundation of China (Grant No. 51779183). DAE was supported by National Science Foundation grants EAR-1426997 and EAR-1812019. The Yellow River Conservancy Commission is sincerely thanked for providing the data used in

this study. We are indebted to Professor Jeffrey A. Nittrouer at Rice University and senior engineer Kairong Wang at the Yellow River Institute of Hydraulic for their insightful suggestions. Yunjin Zhou is thanked for editing Fig. 2 and assisting in data analysis.

References

Alexander, J.S., Wilson, R.C., Green, W.R., 2012. A Brief History and Summary of the Effects of River Engineering and Dams on the Mississippi River System and Delta. 1067084X. U. S. Geological Survey, Reston, VA, United States.

Bi, N., Wang, H.J., Yang, Z.S., 2014. Recent changes in the erosion–accretion patterns of the active Huanghe (Yellow River) delta lobe caused by human activities. Cont. Shelf Res. 90, 70–78.

Chatanantavet, P., Lamb, M.P., Nittrouer, J.A., 2012. Backwater controls of avulsion location on deltas. Geophys. Res. Lett. 39, L01402. https://doi.org/10.1029/ 2011G1050197.

Chu, Z.X., Sun, X.G., Zhai, S.K., Xu, K.H., 2006. Changing pattern of accretion/erosion of the modern Yellow River (Huanghe) subaerial delta, China: based on remote sensing images. Mar. Geol. 227 (1), 13–30.

Coleman, J.M., 1988. Dynamic changes and processes in the Mississippi River delta. Geol. Soc. Am. Bull. 100 (7), 999–1015.

Coleman, J.M., Robert, H.H., Stone, G.W., 1998. Mississippi River Delta: an Overview. J. Coast. Res. 14 (3), 699–716.

Edmonds, D.A., Slingerland, R.L., 2010. Significant effect of sediment cohesion on delta morphology. Nat. Geosci. 3 (2), 105–109.

Edmonds, D.A., Hoyal, D.C.J.D., Sheets, B.A., Slingerland, R.L., 2009. Predicting delta avulsions: implications for coastal wetland restoration. Geology 37 (8), 759–762.

Ganti, V., Chu, Z., Lamb, M.P., Nittrouer, J.A., Parker, G., 2014. Testing morphodynamic controls on the location and frequency of river avulsions on fans versus deltas: Huanghe (Yellow River), China. Geophys. Res. Lett. 41, 7882–7890.

Ganti, V., Chadwick, A.J., Hassenruck-Gudipati, H.J., Lamb, M.P., 2016. Avulsion cycles and their stratigraphic signature on an experimental backwater-controlled delta. J. Geophys. Res. Earth Surf. 121, 1651–1675.

- Hoyal, D.C.J.D., Sheets, B.A., 2009. Morphodynamic evolution of experimental cohesive deltas. J. Geophys. Res. Earth Surf. 114, F02009. https://doi.org/10.1029/2007JF000882.
- Jerolmack, D.J., Swenson, J.B., 2007. Scaling relationships and evolution of distributary networks on wave-influenced deltas. Geophys. Res. Lett. 34, L23402. https://doi. org/10.1029/2007GL031823.
- Kasai, M., Marutani, T., Brierley, G., 2004. Channel bed adjustments following major aggradation in a steep headwater setting: findings from Oyabu Creek, Kyushu, Japan. Geomorphology 62 (3–4). 199–215.
- Lamb, M.P., Nittrouer, J.A., Mohrig, D., Shaw, J., 2012. Backwater and river plume controls on scour upstream of river mouths: Implications for fluvio-deltaic morphodynamics. J. Geophys, Res. Earth Surf. 117, F01002. https://doi.org/10.1029/2011|F002079.
- Nittrouer, J.A., Shaw, J., Lamb, M.P., Mohrig, D., 2012. Spatial and temporal trends for water-flow velocity and bed-material sediment transport in the lower Mississippi River. Geol. Soc. Am. Bull. 124, 400–414.
- Pang, J.Z., Si, S.H., 1979. Evolution of the Yellow River mouth: I. Historical shifts. Oceonologia et Limnologia Sinica 10 (2), 136–141.
- Reitz, M.D., Jerolmack, D.J., Swenson, J.B., 2010. Flooding and flow path selection on alluvial fans and deltas. Geophys. Res. Lett. 37, L06401. https://doi.org/10.1029/2009CI.041985
- Schumm, S.A., Erskine, W.D., Tilleard, J.W., 1996. Morphology, hydrology and evolution of the anastomosing Ovens and King Rivers, Victoria, Australia. Geol. Soc. Am. Bull. 108 (10), 1212–1224.
- Shi, C.X., Zhang, D., 2003. Processes and mechanisms of dynamic channel adjustment to delta progradation: the case of the mouth channel of the Yellow River, China. Earth Surf. Process. Landf. 28 (6), 609–624.
- Sinha, R., 2009. The Great avulsion of Kosi on 18 August 2008. Curr. Sci. 97 (3), 429–433.
 Sinha, R., Sripriyanka, K., Jain, V., Mukul, M., 2014. Avulsion threshold and planform dynamics of the Kosi River in north Bihar (India) and Nepal: a GIS framework. Geomorphology 216, 157–170.
- Syvitski, J.P.M, Saito, Y., 2007. Morphodynamics of deltas under the influence of humans. Glob. Planet. Chang. 57, 261–282.
- van Dijk, M., Postma, Č., Kleinhans, M., 2009. Autocyclic behavior of fan deltas: an analogue experimental study. Sedimentology 56, 1569–1589.
- Wang, K.C., 2010. Evolution and Management of the Yellow River Delta. Yellow River Water Conservancy Press, Zhengzhou (in Chinese).
- Wang, Z.Y., Liang, Z.Y., 2000. Dynamic characteristics of the Yellow River mouth. Earth Surf. Process. Landf. 25 (7), 765–782.

- Wang, B., Xu, Y.J., 2018a. Decadal-scale riverbed deformation and sand budget of the last 500 km of the Mississippi River: insights into natural and river engineering effects on a large alluvial river. I. Geophys. Res. Earth Surf. 123, 874–890.
- Wang, B., Xu, Y.J., 2018b. Dynamics of 30 large channel bars in the Lower Mississippi River in response to river engineering from 1985 to 2015. Geomorphology 300, 31–44.
- Wang, W.Z., Zhang, S.A., Nittrouer, J.A., 2018. A formula for channel roughness for the Yellow River Estuary. Yellow River 40 (12), 4–8 (in Chinese).
- Wu, B.S., Wang, G.Q., Xia, J.Q., Fu, X.D., Zhang, Y.F., 2008a. Response of bankfull discharge to discharge and sediment load in the lower Yellow River. Geomorphology 100 (3), 366–376
- Wu, B.S., Xia, J.Q., Fu, X.D., Zhang, Y.F., Wang, G.Q., 2008b. Effect of altered flow regime on bankfull area of the lower Yellow River, China. Earth Surf. Process. Landf. 33 (10), 1585–1601
- Wu, X., Bi, N., Xu, J., et al., 2017. Stepwise morphological evolution of the active yellow river (Huanghe) delta lobe (1976–2013): dominant roles of riverine discharge and sediment grain size. Geomorphology 292, 115–127.
- Xu, J.X., 2003. A study of sediment delivery by floods in the lower Yellow River. Hydrolog. Sci. I, IAHS 48 (4), 553–566.
- Zeng, Q.H., Zhang, S.Q., Hu, C.H., Yin, X.L., Li, Z.G., Jiao, Y.L., 1997. Engineering Training and Evolution of the Yellow River Delta. Yellow River Water Conservancy Press, Zhengzhou, Henan Province (in Chinese).
- Zhang, Y.F., Zhang, L.Z., Liang, G.T., et al., 2005. Analysis and Comments of Aggradation/degradation Calculation Method Based on Cross-sectional Surveys at the Lower Yellow River. Yellow River Conservancy Press, Zhengzhou, Henan Province (in Chinese).
- Zheng, S., Wu, B.S., Thorne, C.R., Simon, A., 2014. Morphological evolution of the North Fork Toutle River following the eruption of Mount St. Helens, Washington. Geomorphology 208, 102–116.
- Zheng, S., Wu, B.S., Wang, K.C., Tan, G.M., Han, S.S., Thorne, C.R., 2017. Evolution of the Yellow River delta, China: impacts of channel avulsion and progradation. Int. J. Sediment Res. 32, 34–44.
- Zheng, S., Han, S., Tan, G., et al., 2018. Morphological adjustment of the Qingshuigou channel on the Yellow River Delta and factors controlling its avulsion. Catena 166. 44–55.
- Zhou, Y., Huang, H.Q., Nanson, G.C., Huang, C., Liu, G., 2015. Progradation of the Yellow (Huanghe) River delta in response to the implementation of a basin-scale water regulation program. Geomorphology 243, 65–74.